

# UC Santa Barbara

## UC Santa Barbara Previously Published Works

### Title

Discerning molecular-level CO<sub>2</sub> adsorption behavior in amine-modified sorbents within a controlled CO<sub>2</sub>/H<sub>2</sub>O environment towards direct air capture

### Permalink

<https://escholarship.org/uc/item/2v79h67f>

### Journal

Journal of Materials Chemistry A, 12(38)

### ISSN

2050-7488

### Authors

Song, Ah-Young

Young, John

Wang, Jieyu

et al.

### Publication Date

2024-10-01

### DOI

10.1039/d4ta05578k

Peer reviewed

# Discerning molecular-level CO<sub>2</sub> adsorption behavior in amine-modified sorbents within a controlled CO<sub>2</sub>/H<sub>2</sub>O environment towards direct air capture†

Ah-Young Song,<sup>ab</sup> John Young,<sup>c</sup> Jieyu Wang,<sup>a</sup> Sophia N. Fricke,<sup>a</sup> Katia Piscina,<sup>c</sup> Raynald Giovine,<sup>d</sup> Susana Garcia,<sup>c</sup> Mijndert van der Spek<sup>c</sup> and Jeffrey A. Reimer<sup>\*ab</sup>

Sorbents designed for direct air capture (DAC) play a crucial role in the pursuit of achieving net-zero carbon dioxide emissions. This study elucidates CO<sub>2</sub> adsorption from dilute, humidified CO<sub>2</sub> streams onto an amine-modified benchmark DAC adsorbent *via* solid-state NMR spectroscopy. Various NMR techniques, including 1D <sup>1</sup>H MAS, <sup>13</sup>C MAS, 2D <sup>1</sup>H–<sup>13</sup>C HETCOR NMR, and <sup>1</sup>H *R*<sub>2</sub> and *R*<sub>1ρ</sub> relaxometry reveal the impact of CO<sub>2</sub> partial pressure and H<sub>2</sub>O on CO<sub>2</sub> adsorption behavior. We find that CO<sub>2</sub> concentration governs the stepwise formation of ammonium carbamate, carbamic acid, and physisorbed CO<sub>2</sub>, where relative humidity (RH) at a desired low (<400 ppm) CO<sub>2</sub> loading affects total CO<sub>2</sub> uptake. The relaxation studies reveal the cooperative or competitive nature of H<sub>2</sub>O–CO<sub>2</sub> sorption in CO<sub>2</sub>-dilute humid gas, and in particular polymer swelling upon humidification. From those results, we demonstrate that the observed absorption capacity enhancement by humidity is caused by pore opening due to sorbent swelling, and not by bicarbonate formation. This NMR-discerned speciation provides insights into sorption behavior at different RHs in dilute CO<sub>2</sub> gas streams, simulating real-world atmospheric conditions, and governs the design of efficient and adaptable material-process combinations for solid sorbent DAC.

## Introduction

Direct air capture (DAC) is a promising technology towards net-zero carbon dioxide emissions and beyond,<sup>1</sup> notable for its independence from point source emission locations and its ability to operate without the need for costly infrastructure, such as long CO<sub>2</sub> pipelines.<sup>2</sup> Particularly, DAC is identified as a critical tool to address hard-to-abate emissions, which are challenging to eliminate due to technical limitations, economic constraints, or considerations of social justice.<sup>3</sup> It also enables the net-negative emission scenarios needed to keep global warming under 1.5 °C or 2 °C, aligning with international climate targets.<sup>3</sup> One DAC technology currently being scaled is

solid sorbent DAC, where air is contacted with a solid porous material that is regenerated using elevated temperature, vacuum, or both. A crucial aspect of solid sorbent DAC is the sorbent's capability to efficiently extract CO<sub>2</sub> from a humid and ultradilute-CO<sub>2</sub>, *i.e.* 400 ppm, stream, in contrast to the CO<sub>2</sub>-rich (*e.g.* 4–20%) streams targeted with the point source CO<sub>2</sub> capture.<sup>4</sup>

Effective DAC sorbents must meet essential criteria such as high CO<sub>2</sub> capacity, high selectivity over other components found in air, rapid sorption/desorption kinetics, thermal/chemical stability, cost-effective regeneration, and affordability.<sup>4</sup> These inherent material characteristics of the sorbents are directly linked to the CO<sub>2</sub> adsorption mechanisms. Additionally, CO<sub>2</sub> adsorption is influenced by combined external environmental factors and ambient conditions such as temperature, CO<sub>2</sub> partial pressure, the presence of water vapor in the air, as well as other competing gases including N<sub>2</sub>, and O<sub>2</sub>.<sup>5,6</sup> Indeed, the concentration of water is typically orders of magnitude higher than the concentration of CO<sub>2</sub> in ambient air, and thus water may compete with CO<sub>2</sub> for adsorption sites and/or enhance CO<sub>2</sub> adsorption *via* physical or chemical mechanisms. Consequently, environmental factors can fundamentally

<sup>a</sup>Department of Chemical and Biomolecular Engineering, University of California, Berkeley, CA 94720, USA. E-mail: reimer@berkeley.edu

<sup>b</sup>Materials Sciences Division, Lawrence Berkeley National Laboratory, Berkeley, CA 94720, USA

<sup>c</sup>Research Centre for Carbon Solutions, Heriot-Watt University, Edinburgh, EH14 4AS, UK

<sup>d</sup>College of Chemistry Pines Magnetic Resonance Center - Core Facility, University of California, Berkeley, CA 94720, USA

1 alter the adsorption amount and dynamics of a given material, thereby obfuscating field operation and control of DAC units.

Amongst the many potential sorbent materials, amine-modified sorbents are widely studied for DAC due to their high CO<sub>2</sub> capacity at ultradilute-CO<sub>2</sub> concentrations and their high selectivity for CO<sub>2</sub> over N<sub>2</sub> and H<sub>2</sub>O. As a result, they are the only class of adsorbents used in DAC processes at scale today.<sup>7</sup> Thus, there has been some effort in the past two decades to study the impact of humidity on equilibrium CO<sub>2</sub> uptake in amine-modified adsorbents. There remains, however, challenges to validate working hypotheses for sorption dynamics with reliable experimental studies.<sup>2,8-12</sup> Generally, it appears that the CO<sub>2</sub> uptake is enhanced in the presence of water at low relative humidities, yet uptake becomes less favorable at higher humidity levels. Previous studies have attributed enhanced CO<sub>2</sub> adsorption capacity to the formation of ammonium bicarbonate over ammonium carbamate, thereby doubling the potential stoichiometry of adsorption.<sup>13</sup> However, this hypothesis has proven difficult to affirm given that the prolonged timescales required to form bicarbonate are not consistent with observed CO<sub>2</sub> adsorption.<sup>14,15</sup> Some studies have either not observed bicarbonate formation or reported only a very subtle presence of this species in humid CO<sub>2</sub> environments.<sup>16-18</sup> Instead, these studies have reported the formation of other major species, such as ammonium carbamate. Nevertheless, previous research on these species still does not entirely account for the observed enhanced CO<sub>2</sub> uptake. In-depth experimental examination of water-CO<sub>2</sub> co-adsorption mechanisms in amine-functionalized adsorbents is largely missing, and therefore the exact nature of the observed adsorption phenomena is yet to be well understood. Absent a molecular understanding relating air composition to process behavior, DAC process performance is compromised, which has large implications for DAC plant siting decisions, as well as design and optimization of processes and materials.<sup>5,6</sup>

In this study, we clarify why and how H<sub>2</sub>O impacts CO<sub>2</sub> adsorption in amine functionalized polymer resins. Lewatit® VP OC 1065 is used as an off-the-shelf benchmark sorbent as it exhibits a higher CO<sub>2</sub> adsorption capacity compared to other resins having the same supportive material.<sup>19</sup> Previous research into this material has provided analyses of pore structure,<sup>20</sup> concentrations of functional groups,<sup>20</sup> oxidative degradation phenomenology,<sup>21,22</sup> material regeneration,<sup>20</sup> thermal and chemical stability over long-term exposure,<sup>23</sup> and performance in CO<sub>2</sub> and H<sub>2</sub>O sorption.<sup>20</sup> Additionally, researchers have investigated the molecular interactions between this sorbent and CO<sub>2</sub> using DRIFTS FTIR spectroscopy; they suggested formation of carbamate/carbamic acid and possibly bicarbonate under dry conditions, yet they concluded that the exact nature of captured species was undetermined.<sup>20</sup> Computational investigations have examined preferred adsorption processes in the presence of water, discussing direct amine-H<sub>2</sub>O interactions and amine catalyzed formation of carbamic acid,<sup>24</sup> suggesting that carbamic acid formation is the preferred pathway. Previous studies on CO<sub>2</sub> adsorption capacity have shown that water does not impede CO<sub>2</sub> adsorption between 0-60% RH;<sup>10</sup> however, the role of water in adsorption may vary with changes

1 in partial pressure.<sup>25</sup> Nevertheless, research to understand adsorption pathways in the presence of water remains limited. We surmise that a deeper molecular understanding of water/amine/CO<sub>2</sub> interactions is currently lacking, and it is key to the design of sorbent-based DAC processes.

Expanding on those earlier discoveries, this study focuses on elucidating the interaction of amine-functionalized polymer resins with CO<sub>2</sub> under both dry and wet conditions using <sup>13</sup>C and <sup>1</sup>H solid-state NMR (ssNMR) spectroscopy. By varying CO<sub>2</sub> partial pressure and relative humidity, this NMR study identifies and quantitates chemisorbed species to assess enhanced or reduced CO<sub>2</sub> adsorption capacity. We find conclusive evidence that bicarbonate is not formed under humid conditions, contrary to earlier hypotheses. Furthermore, the CO<sub>2</sub> adsorption reaction within Lewatit® VP OC 1065 is primarily dictated by the CO<sub>2</sub> partial pressure during adsorption. NMR relaxometry reveals polymer pore swelling at higher humidity levels, and this modulates the competitive and cooperative adsorption of H<sub>2</sub>O and CO<sub>2</sub>. These findings allow the adjustment of current co-adsorption models to enhance their predictive capabilities and provide more robust insights on adsorbent performance.

## Results and discussion

### Impact of CO<sub>2</sub> partial pressure on adsorption (under dry conditions)

The material Lewatit® VP OC 1065, featuring primary amine groups presumed to serve as chemisorption sites for CO<sub>2</sub>, was selected as a prototypical material to investigate the role of CO<sub>2</sub> partial pressure in its adsorption mechanism for DAC application. Activated materials were loaded at varying <sup>13</sup>CO<sub>2</sub> partial pressures (*p*CO<sub>2</sub> = 1000, 35 or 8 mbar) under dry conditions and analyzed using solid-state NMR spectroscopy. The <sup>13</sup>C CPMAS spectra presented in Fig. 1 demonstrate distinct chemisorption peaks between 155-170 ppm at various CO<sub>2</sub> loadings, with at least two discernible environments at 164 and 160 ppm. Additionally, Fig. S1a† employs direct polarization <sup>13</sup>C DPMAS and reveals a physisorption peak at 125 ppm, observed only at approximately 1000 mbar. Detailed spectral analysis (Fig. S1b†) further describes the characteristic peaks of the sorbent materials at 40-50 ppm, 120-130 ppm, and 140-150 ppm.

To better identify the different chemisorbed species, 2D <sup>1</sup>H-<sup>13</sup>C Heteronuclear Correlation (HETCOR) NMR was employed to probe the through space close proximities between <sup>1</sup>H and <sup>13</sup>C nuclei. <sup>13</sup>C-<sup>1</sup>H FSLG-HETCOR, where the FSLG protocol enhances the <sup>1</sup>H resolution in 2D HETCOR spectra, are shown in Fig. 2. This 2D correlation map clearly demonstrates variation in the formation of ammonium carbamate and carbamic acid across different CO<sub>2</sub> loadings. At a CO<sub>2</sub> partial pressure (*p*CO<sub>2</sub>) of 35 mbar, the <sup>13</sup>C resonance at 164 ppm is associated exclusively with NH (3.7 ppm) and NH<sub>3</sub><sup>+</sup> (7.8 ppm) (Fig. 2a). In contrast, at approximately 1000 mbar (Fig. 2b), the resulting <sup>13</sup>C spectrum can be deconvoluted into three environments: I at 164 ppm, II at 161.1 ppm, and III at 159.2 ppm. The <sup>1</sup>H projections for each <sup>13</sup>C environment reveal different close proximities between carbons and protons (Fig. 2c). The three

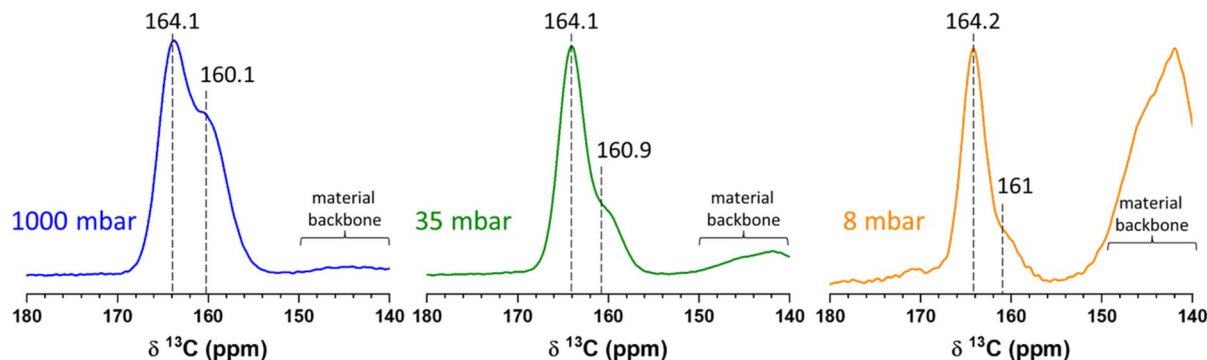


**Fig. 1**  $^{13}\text{C}$  solid-state CPMAS (contact time 2 ms) NMR of  $\text{CO}_2$  adsorbed at various pressures (1000 mbar in blue, 35 mbar in green or 8 mbar in orange) within Lewatit® VP OC 1065. Signals observed between 140 to 150 ppm originate from the backbone in Lewatit® VP OC 1065, where not affected by  $\text{CO}_2$  adsorption.

$^{13}\text{C}$  resonances at 164, 161.1, and 159.2 ppm (environment I, II, and III, respectively) correlate with  $^1\text{H}$  signals of NH at 3.7 ppm and  $\text{NH}_3^+$  at 7.8 ppm. In addition, the  $^{13}\text{C}$  site at 159.2 ppm (environment III) correlates with COOH at 15.1 ppm, while the  $^{13}\text{C}$  site at 161.1 ppm (environment II) exhibits a weaker correlation with COOH (Fig. 2c) than environment III at 159.2 ppm. Based on this observation, we surmise that environment II may not be a distinct species but rather a mixed species comprising both ammonium carbamate and carbamic acid; this observation is consistent with previous NMR studies of melamine porous network polymer adsorbents.<sup>26</sup> These results demonstrate that ammonium carbamate ( $\text{NHCOO}^-$ ) is dominantly formed at  $p\text{CO}_2 = 35$  mbar, while both ammonium carbamate ( $\text{NHCOO}^-$ ) and ammonium carbamic acid ( $\text{NHCOOH}$ ) contribute to  $\text{CO}_2$  adsorption at  $p\text{CO}_2 = 1000$  mbar.

Speciation of the local  $^{13}\text{C}$  environment at I (164 ppm) and III (159.2 ppm) is further clarified by exploiting the  $^{13}\text{C}$  chemical shift anisotropy (CSA) of these sites. While the CSA is typically averaged out during MAS, at slower spinning speeds the spinning sidebands of the NMR spectra are observed and these sidebands may be used to estimate the CSA for each isotropic

chemical shift.<sup>27</sup> The  $^{13}\text{C}$  CSA associated with each chemical shift is shown in Fig. S2† and can be used to distinguish between protonated ( $\text{COOH}$ ) and deprotonated ( $\text{COO}^-$ ) species (see ESI for details†).<sup>28,29</sup> This analysis corroborates the HETCOR spectra, validating the identification of ammonium carbamate (site I) and carbamic acid (site III). Furthermore, a significant decrease in resonance at 159 ppm in Fig. S3,† detected after exposing the  $\text{CO}_2$ -loaded materials at 1000 mbar to the ambient air, provides clear evidence for carbamic acid to be associated with environment III; this moiety is an unstable species in the air.

In summary, the variations in  $\text{CO}_2$  partial pressure determine the interaction mechanisms with Lewatit® VP OC 1065 in the absence of water. Fig. 3 illustrates that the adsorption occurs as a stepwise process with respect to the partial pressure of  $\text{CO}_2$ : at low  $\text{CO}_2$  loading, adsorption is mainly governed by the formation of ammonium carbamate; as the  $\text{CO}_2$  loading gradually increases, the formation of carbamic acid accompanies the formation of ammonium carbamate. At higher  $\text{CO}_2$  pressures, we surmise that mixed ammonium carbamate and carbamic acid pairs appear. Moreover, physisorption appears

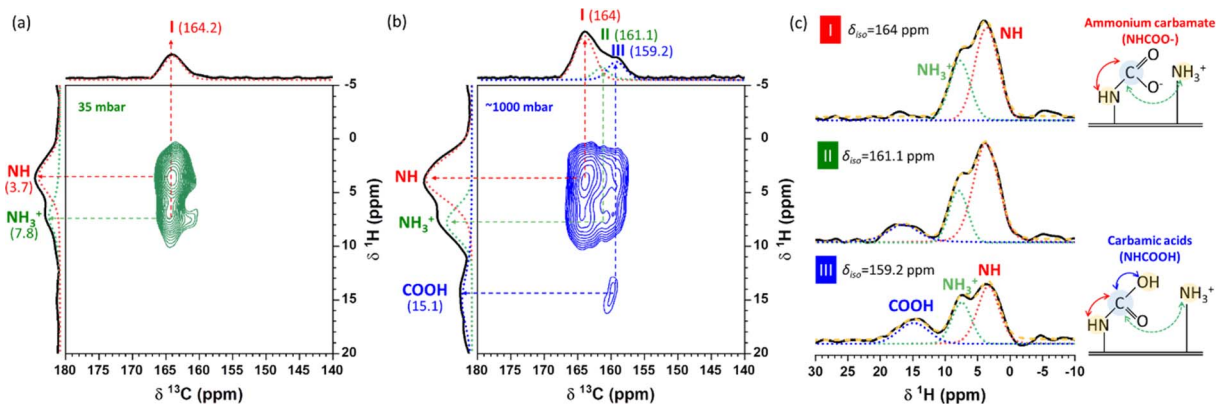


**Fig. 2**  $2\text{D } ^1\text{H}-^{13}\text{C}$  FSLG-HETCOR spectra recorded with a contact time of 50  $\mu\text{s}$  for Lewatit® VP OC 1065 loaded with (a) 35 mbar or (b) approx. 1 bar of  $^{13}\text{CO}_2$ . The chosen contact time of 50  $\mu\text{s}$  highlights protonated carbon sites. (c) Individual  $^1\text{H}$  projection for each  $^{13}\text{C}$  environment (I, II, and III in (b)) observed in the 2D spectrum in (b) at approximately 1 bar of  $^{13}\text{CO}_2$  are deconvoluted with colored dashed lines: NH (red),  $\text{NH}_3^+$  (green), and COOH (blue).

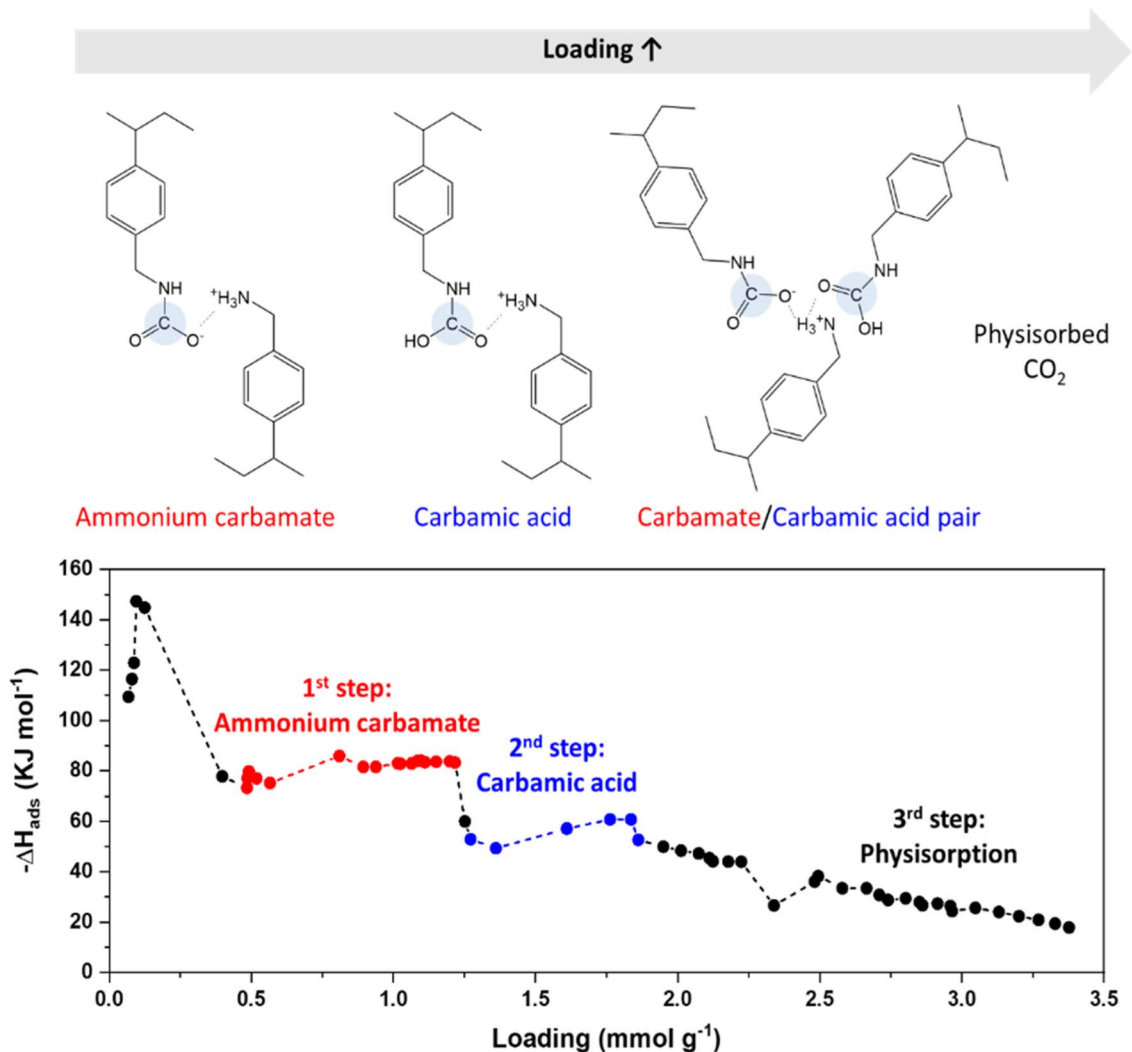


Fig. 3 Proposed stepwise CO<sub>2</sub> adsorption process at increasing CO<sub>2</sub> partial pressures: illustration of molecular structures (top) and the computed isosteric heat of adsorption (bottom). Isosteric heats of adsorption ( $-\Delta H_{\text{ads}}$ ) calculated from the isotherm data described previously (reproduced from ref.25 with permission from the Royal Society of Chemistry).

exclusively at the highest CO<sub>2</sub> loading (1000 mbar). These NMR analyses are consistent with previously computed isosteric heats of adsorption ( $-\Delta H_{\text{ads}}$ ) under dry conditions as a function of CO<sub>2</sub> loading (Fig. 3, bottom).<sup>25</sup> These heats of adsorption reveal a step-wise change with CO<sub>2</sub> loading, and the present NMR results provide a basis for their molecular interpretation.

#### Co-adsorption of H<sub>2</sub>O and CO<sub>2</sub>

Water vapor plays a complex role in CO<sub>2</sub> adsorption, and can serve both as a facilitator and an inhibitor of adsorption, depending on the environmental conditions and on the type of adsorbent used.<sup>30</sup> Acting as a free base, water can initiate various reaction pathways such as hydrolysis of carbamates to bicarbonate, as reported in both theoretical calculation and NMR studies on aqueous amine solution.<sup>31,32</sup> Additionally, Grand Canonical Monte Carlo (GCMC) studies showed the hydration of materials can generate additional adsorption active sites at the terminal water molecules in MIL-101,<sup>33</sup>

boosting CO<sub>2</sub> adsorption, especially under low-pressure mixed gases. Conversely, water can also have detrimental effects on CO<sub>2</sub> adsorption by competing for adsorption sites. This competition can arise when water molecules weaken the interaction between CO<sub>2</sub> and the adsorbent surface through *e.g.*, a reduction in the electric field,<sup>34</sup> or dominate the binding occupancy due to their strong dipole moments.<sup>35</sup> The formation of water clusters can further obstruct CO<sub>2</sub> adsorption.<sup>36</sup> We utilized the apparatus shown in Fig. S4† to systematically investigate the influence of water on CO<sub>2</sub> adsorption onto Lewatit® VP OC 1065. Activated materials were loaded with varying amounts of water to establish relative humidities (RHs) of 0%, 30%, and 80% (labelled RH0, RH30, and RH80, respectively) at a controlled CO<sub>2</sub> concentration of approximately 0.15 mbar (equivalent to 150 ppm). The chosen CO<sub>2</sub> concentration, set below atmospheric levels (~400 ppm), aims to observe potentially maximized adsorption effects and to maximize the detection sensitivity for all species, including potential minor



species. It has been previously reported that adsorption efficiency doubled at 0.2 mbar CO<sub>2</sub>, 25 °C, and increased more than 2.5 times at 0.1 mbar CO<sub>2</sub>, 70 °C, and decrease as the pressure increases.<sup>25</sup> This approach allowed us to probe the molecular interactions at low partial pressure under different humidity conditions *via* solid-state NMR.

Water adsorption may not be easily discernible in <sup>1</sup>H NMR because its chemical shift at 4.5 ppm overlaps with the broader <sup>1</sup>H NMR signals from Lewatit® VP OC 1065, which displays overlapping peaks spanning from 0 to 10 ppm. Nevertheless, Fig. 4a reveals a gradual increase in the H<sub>2</sub>O signal intensity at 4.5 ppm as the RH increases, and an intense signal is observed for H<sub>2</sub>O at 80% RH. This indicates that higher RH results in increased water adsorption. More interestingly, for CO<sub>2</sub> adsorption across all RHs, a single resonance is consistently observed around 164.5 ppm as a chemisorption in <sup>13</sup>C CPMAS NMR spectra (Fig. 4b). The formation of a chemisorbed species

around 164.5 ppm is confirmed by 2D <sup>13</sup>C-<sup>1</sup>H HETCOR (Fig. 4c), demonstrating clear correlations between the <sup>13</sup>C site at 164.5 ppm with proton signals emanating from NH and NH<sub>3</sub><sup>+</sup> groups. This establishes that ammonium carbamate forms at the tested CO<sub>2</sub> partial pressure, regardless of the RH percentage. However, water can dissolve CO<sub>2</sub> under humid conditions and lead to the formation of moieties such as bicarbonate or carbonate.<sup>31,37</sup> Those dissolved moieties may experience high mobility, and thus may remain undetected in CPMAS NMR studies.<sup>38,39</sup> Therefore, <sup>13</sup>C direct excitation was utilized to discern the presence of mobile dissolved species. The single resonance near 164.5 ppm (highlighted area in Fig. 5a) and the lack of additional resonances near it clearly demonstrate the exclusive formation of ammonium carbamate across all conditions, both dry and wet, at the controlled *p*CO<sub>2</sub>.

It is worth noting that only when the partial pressure of CO<sub>2</sub> greatly exceeds 400 ppm atmospheric levels do we observe

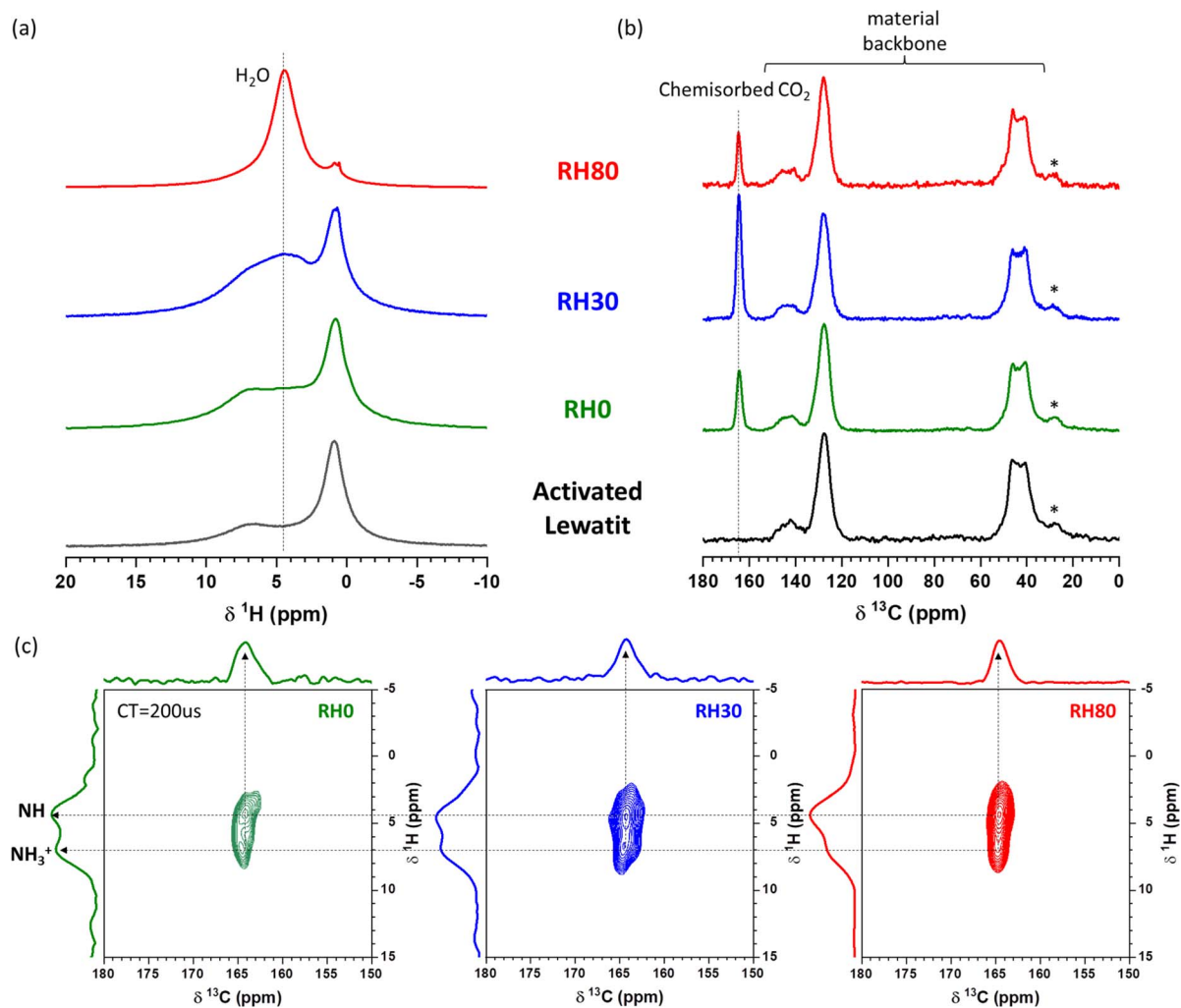
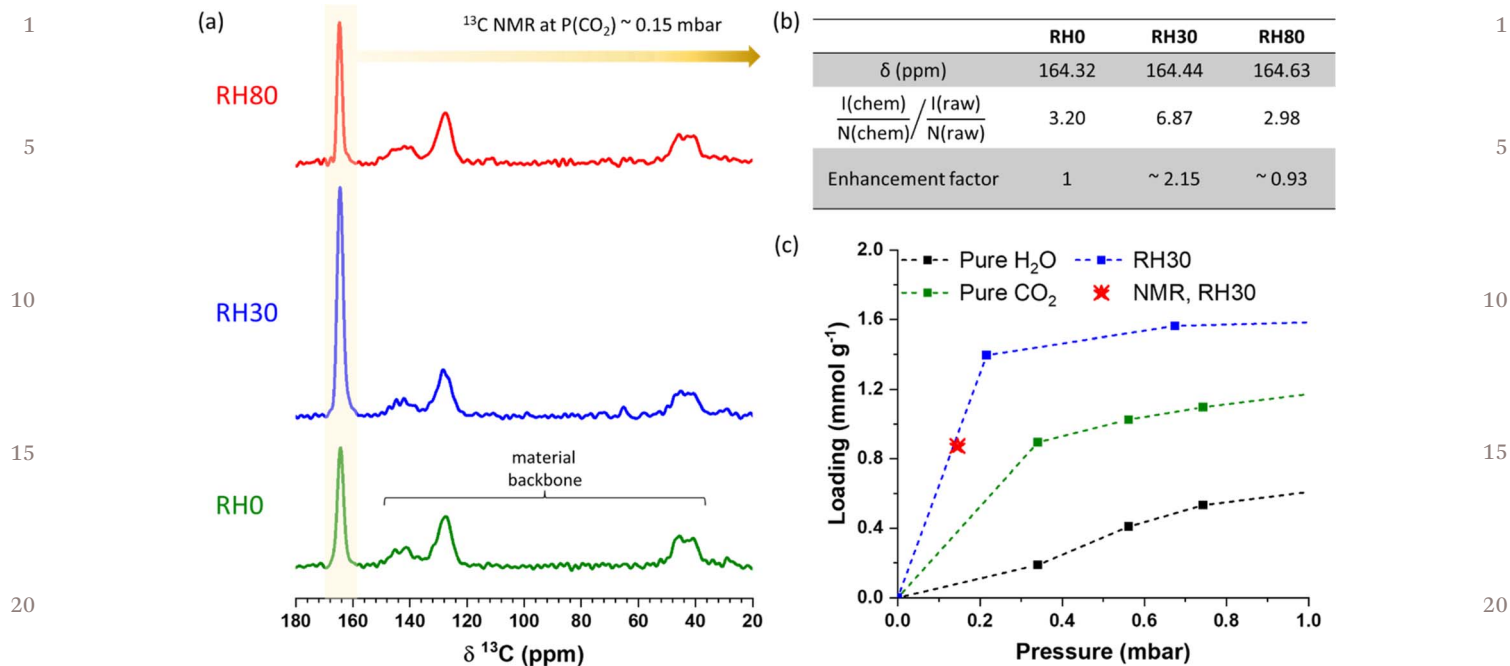


Fig. 4 Solid-state MAS NMR spectra of Lewatit® VP OC 1065 dosed with co-adsorption (N<sub>2</sub>, CO<sub>2</sub>, and H<sub>2</sub>O) at low *p*CO<sub>2</sub> with variable RHs (RH0, RH30, and RH80). (a) <sup>1</sup>H DEPTH NMR; (b) <sup>13</sup>C CPMAS NMR with 200 μs of contact time; (c) <sup>13</sup>C-<sup>1</sup>H FSLG-HETCOR 2D spectra with 200 μs of contact time. Activated Lewatit refers to a state where sample pretreatment (high vacuum) lead to no adsorbed species. In <sup>13</sup>C CPMAS NMR spectra, \* indicates spinning sideband and signals at 40–50 ppm, 120–130 ppm, and 140 to 150 ppm arise from the backbone in Lewatit® VP OC 1065, where not affected by CO<sub>2</sub> adsorption.



**Fig. 5** Quantitative  $\text{CO}_2$  adsorption at various relative humidities. (a) Solid-state  $^{13}\text{C}$  NMR obtained by direct excitation under MAS on samples exposed to a mixture gas  $\text{N}_2 + \text{CO}_2 + \text{H}_2\text{O}$  at  $25^\circ\text{C}$  with RH0 (bottom, green), RH30 (middle, blue), and RH80 (top, red). (b) Tabulated values of quantified  $\text{CO}_2$  adsorption corresponding to the NMR spectra shown in (a). In table,  $I$  (chem or raw) represents the integral area associated with chemisorbed species or sorbent itself in the spectra, and  $N$  (chem or raw) denotes the number of carbons associated with chemisorbed species or sorbent itself. (c) Comparison of the adsorbed  $\text{CO}_2$  obtained from NMR ( $\text{N}_2 + \text{CO}_2 + \text{H}_2\text{O}$ ) with the isotherm experiments  $\text{CO}_2$ , RH30 ( $\text{CO}_2 + \text{H}_2\text{O}$ ), and water at  $25^\circ\text{C}$ . Isotherm experiments were described previously and reproduced from ref.<sup>25</sup> with permission from the Royal Society of Chemistry.

species other than ammonium carbamate. The 2D  $^{13}\text{C}$ - $^1\text{H}$  HETCOR spectra recorded on the 80% RH and 1 bar  $p\text{CO}_2$  sample suggests the formation of other interactions among  $\text{CO}_2$ ,  $\text{H}_2\text{O}$ , and the material (Fig. S5<sup>†</sup>). This spectrum suggests the possibility of ammonium carbamate and urea presence at high  $\text{CO}_2$  loadings as indicated by the correlations at  $\delta(^{13}\text{C}) = 161$  and  $158.1$  ppm, respectively. The observed correlation remains challenging to identify a particular species without ambiguities and a more in-depth study would be needed to understand their species formed at high  $p\text{CO}_2$  and high RHs.

Following the detection of chemisorbed species in the presence of water at low  $\text{CO}_2$  loading, further analysis elucidates the impact of  $\text{H}_2\text{O}$  on  $\text{CO}_2$  adsorption capacities through quantitative analysis of the spectra shown in Fig. 5. The quantification of adsorbed  $\text{CO}_2$  was estimated from the ratios of integrated areas of the resonance corresponding to chemisorbed  $\text{CO}_2$  to that associated with the polymer material. This approach allows for the determination of an enhancement factor,<sup>25</sup> simplifying the comparison of adsorbed  $\text{CO}_2$  under different conditions relative to that under dry conditions. Our analysis shows that the adsorbed  $\text{CO}_2$  doubles at 30% RH compared to the dry condition (0% RH). In other words, water aids in  $\text{CO}_2$  adsorption at 30% RH by enhancing the formation of ammonium carbamate, but this increase does not manifest at 80% RH. Estimated  $\text{CO}_2$  adsorption at 30% RH from NMR results aligns with the adsorbed  $\text{CO}_2$  calculated at the corresponding pressure from the isotherm experiments conducted

previously (Fig. 5c).<sup>25</sup> This finding is also in accordance with the previous isotherm experiments at different RHs that showed a two-fold increase in  $\text{CO}_2$  adsorption at 30% RH and a subsequent small reduction in adsorption as RH increases.<sup>25</sup>

### NMR relaxometry to explore water impact

The NMR results above suggest that the presence of water does not yield additional chemical bonding or reactions between  $\text{CO}_2$  and the sorbents at low partial pressures of  $\text{CO}_2$ . Nevertheless, we find that variation in relative humidities increases the total  $\text{CO}_2$  uptake at 30% RH, but not at 80% RH. We surmise that this effect arises from changes in the properties of the resins with hydration and/or molecular dynamics between guest molecules and sorbents. We deployed  $^1\text{H}$  NMR relaxation studies to examine these questions upon water adsorption. The changes in  $^1\text{H}$  NMR relaxation rates indicate a change in the correlation times ( $\tau_c$ ), which characterize motion of protons (e.g. a shorter correlation time indicates faster proton motion). These constructs derive from the original Bloembergen-Pound-Purcell (BPP) theory and have been further elaborated in subsequent NMR treatises.<sup>40,41</sup>

While it is expected that polymer can swell with adsorbates,  $^1\text{H}$  NMR relaxation provides insight into the expansion behavior of polymer resin pores during water adsorption. Particularly, the spin-spin relaxation ( $R_2 = 1/T_2$ ) measurement presents a well-established relationship between transverse relaxation rates and physical characteristics of porous media through

exchange between unbound and sorbent-bound states, as presented in eqn S1.<sup>†42–44</sup> Thus, Fig. 6 and S6<sup>†</sup> shows two well-separated distributions given by water molecules within the pores (pore-confined H<sub>2</sub>O) and those outside the pores (free H<sub>2</sub>O), at least when water is beyond the saturation point. Since  $R_2$  is proportional to correlation time, free H<sub>2</sub>O with faster molecular motion characterized by shorter correlation time, results in lower  $R_2$  relaxation rates (longer  $T_2$  relaxation times). The time evolution of these  $R_2$  profiles following water adsorption indicates an approximate 8% decrease in the transverse relaxation rates ( $R_2$ ) of pore-confined water (Fig. 6b). We thus conclude that there is a discernible surface-to-volumetric expansion of the pores by  $\approx 8\%$  with long exposure to water, *i.e.*, polymer swelling. The specific, time-evolving shapes of pores are difficult to measure directly and are not revealed by this type of relaxation analysis. A detailed study, however, of parameters such as tortuosity as a function of water adsorption measured *via* PFG NMR would assist in connecting pore expansion to specific geometric changes in the pores. Such studies would provide further insight into mass transfer kinetics of sorption.

Polymer swelling upon water adsorption is further confirmed by  $R_2$  measurements using heavy water (D<sub>2</sub>O), highlighting proton signals from the polymer sorbent and not the adsorbed water. This is demonstrated through two complementary experiments: one varying over time with saturated D<sub>2</sub>O adsorption and the other varying with RH levels. In both experiments, a decrease in  $R_2$  indicates faster local motion (shorter correlation times) of polymer, as explained by BPP theory. The time variant  $R_2$  profiles (Fig. S6c and d<sup>†</sup>) show a noticeable decrease in  $R_2$  with saturated D<sub>2</sub>O adsorption. Although precise analysis with D<sub>2</sub>O is limited by a low signal-to-noise ratio and a complicated  $R_2$  distribution as seen *via* Inverse Laplace Transform (ILT) analysis, we nevertheless see adsorbed water as “lubricating” local chain motion in the Lewatit® VP OC 1065, consistent with studies of other polymers.<sup>45</sup> Furthermore, RH variant measurements reveal a clear decrease in  $R_2$  as RH

levels increase by comparing the slopes of each signal decay without ILT analyses (Fig. 7a). While estimating the  $R_2$  value from these measurements encounters limitations such as signal loss during the initial echo period, these changes suggest that the incorporation of D<sub>2</sub>O molecules into the sorbent increases local motions of polymer segments,<sup>46</sup> characterized by shorter correlation times (decreased  $R_2$  rates) for protons specific to the polymer. The gradual decrease in  $R_2$  as RH level increases indicates enhanced polymer segmental mobility of the sorbent,<sup>46</sup> a “lubrication” that likely enhances CO<sub>2</sub> adsorption by enabling easier access of guest molecules to adsorption sites. This increase in polymer mobility with RH level is not limited to our chosen sorbent but has also been observed in PEI:Al<sub>2</sub>O<sub>3</sub>, using fluorescence and NMR characterizations.<sup>46</sup>

These differing  $R_2$  experiments have been tailored to observe the system of interest from different perspectives. The low magnetic field measurement is highly sensitive to protons in water while it is less sensitive to protons in sorbent. To complement a low signal-to-noise ratio with D<sub>2</sub>O measurement at low magnetic field, the experiments at high magnetic fields are conducted to probe the signal directly from the sorbent itself.

Spin-lattice relaxation serves as a further guide to understanding how water interacts with the adsorption properties of Lewatit® VP OC 1065 during water adsorption. Here, we choose to use proton NMR spin-lattice relaxation rates in the rotating frame ( $R_{1\rho} = T_{1\rho}^{-1}$ ), measured under a spin-lock field ( $B_{sl}$ ). This measurement is chosen because it allows to detect bound water motion at mid-kHz range.<sup>45</sup> For very slow motion ( $\omega_1\tau_c \gg 1$ ),  $R_{1\rho}$  is inversely proportional to correlation time. Specifically, faster motion with shorter correlation time increases  $R_{1\rho}$  (shorter  $T_{1\rho}$  relaxation times) as given by BPP theory. Fig. 8 isolates humidity effects on the relaxation mechanisms using only N<sub>2</sub> and D<sub>2</sub>O (or H<sub>2</sub>O). The bound water motion is observed in Fig. 8b, showing a pronounced increase in  $R_{1\rho}$  with increasing humidity when using H<sub>2</sub>O, whereas  $R_{1\rho}$  remains unchanged when using D<sub>2</sub>O (as presented in Fig. 8a).

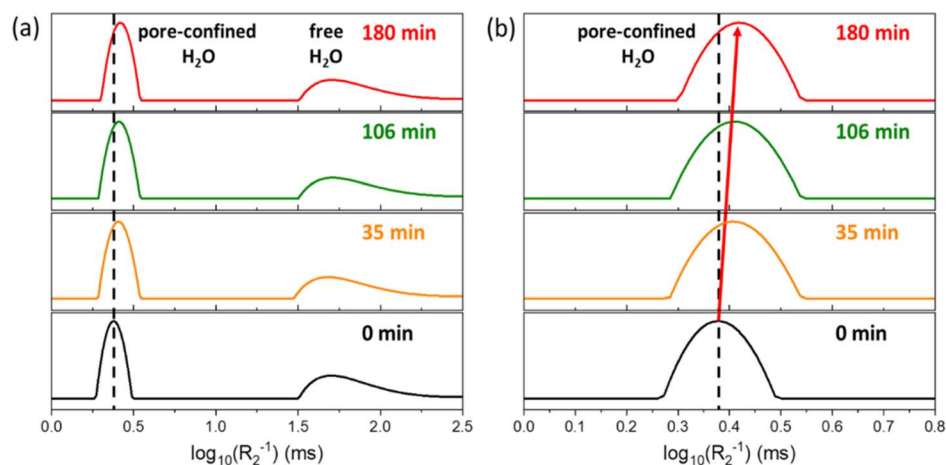


Fig. 6 Changes in transverse relaxation rates ( $R_2^{-1} = T_2$ ) of water saturated within material, measured at a resonant <sup>1</sup>H frequency of 13.11 MHz. (a)  $R_2$  distribution interpreted as pore-confined H<sub>2</sub>O (faster  $R_2$ , *i.e.* shorter  $T_2$ ) and free H<sub>2</sub>O (slower  $R_2$ , *i.e.* longer  $T_2$ ); (b) magnified view of (a), highlighting the changing  $R_2$  distribution of pore-confined H<sub>2</sub>O. Dashed black and solid red lines are a guide to the eye.



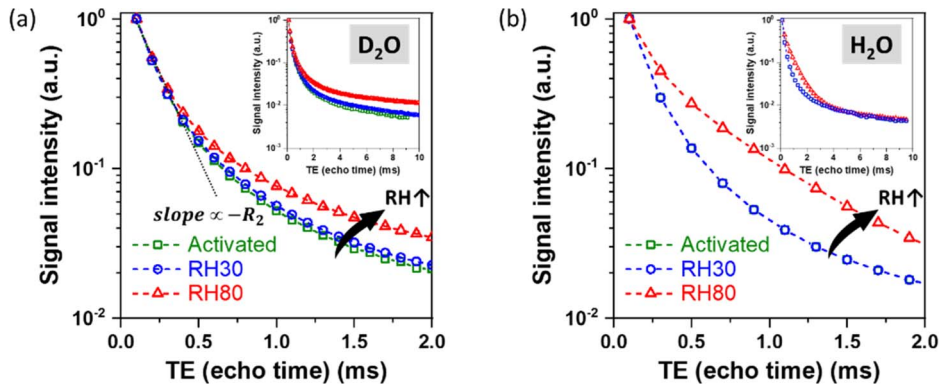


Fig. 7  $^1\text{H}$  NMR relaxation decay curves obtained at 9.4 T of activated and water vapor (including  $\text{N}_2$ , using either (a)  $\text{D}_2\text{O}$  or (b)  $\text{H}_2\text{O}$ ) adsorbed materials at 25  $^\circ\text{C}$  with RH30, and RH80 for  $R_2 = (1/T_2)$  relaxations. Considering potential deuterium exchange in polymer, the data presented in  $\text{D}_2\text{O}$  is used after reactivating  $\text{D}_2\text{O}$  adsorbed sample in (a). Measurements with activated and RH30 in (b) are overlapped in the graph.

Consequently, in this slow motional timescale, the higher  $R_{1p}$  observed with increased RH level suggests faster water molecular motion. This trend is shown as a steeper slope and persists also in experiments performed with co-adsorption of  $\text{CO}_2$ , where  $R_{1p}$  also increases with RH level (see Fig. S7b $\dagger$ ). These results suggest that bound water motion is also “lubricated” by increased relative humidity.

Further, at 30% RH, the relaxation measurements of  $R_{1p}$  and  $R_2$  reveal different response to the faster correlation time of water molecular motion. While the faster correlation time affects  $R_{1p}$  as depicted in Fig. 8b,  $R_2$  shows minimal change even under conditions where  $\text{H}_2\text{O}$  contributes to relaxation in Fig. 7b. This demonstrates that motion of bound water adsorbed at 30% RH is sensitively detected by  $R_{1p}$ , and reflects changes in the correlation times for local water motion at millisecond timescales (kilohertz frequencies); however, it is hardly detected by  $R_2$ , which can detect microsecond (MHz) frequencies and zero-frequency. Thus, this lack of influence on  $R_2$  can imply that the water adsorbed at up to 30% RH is tightly bound to the sorbent or includes a few additional layers of water, which do not significantly affect  $R_2$  measurements. The water protons in both scenarios may not have sufficient

freedom to contribute to  $R_2$  relaxation. Therefore,  $R_{1p}$  is more effective than  $R_2$  in discerning motion of bound water at this humidity level.

As RH level increases from 30% RH to 80% RH, it is important to note that  $R_2$  begins to respond to faster correlation times, becoming sensitive to changes in water molecular motion. A less steep slope in Fig. 7b indicates a noticeable reduction in the  $R_2$  relaxation rate, alongside an increase in  $R_{1p}$  shown by a steeper slope (Fig. 8b). Both relaxation rates reflect a response to the faster motional correlation time, consistent with enhanced molecular mobility due to the adsorption of additional water molecules. This suggests that the water adsorption extends beyond the tightly bound state, which  $R_2$  cannot clearly detect at 30% RH, and likely involves multiple layer adsorption and potentially progressing to capillary water condensation, yielding increased mobility. For the sorbents exposed at 80% RH with  $\text{CO}_2$ , a consistent trend is observed where  $R_{1p}$  increases and  $R_2$  decreases as RH level rises (see Fig. S7 $\dagger$ ). Furthermore, this enhanced water adsorption at 80% RH is corroborated by the well-resolved and intense signal around 4.5 ppm attributed to bulk water in Fig. 4a. This increased water content within pores may block potential  $\text{CO}_2$

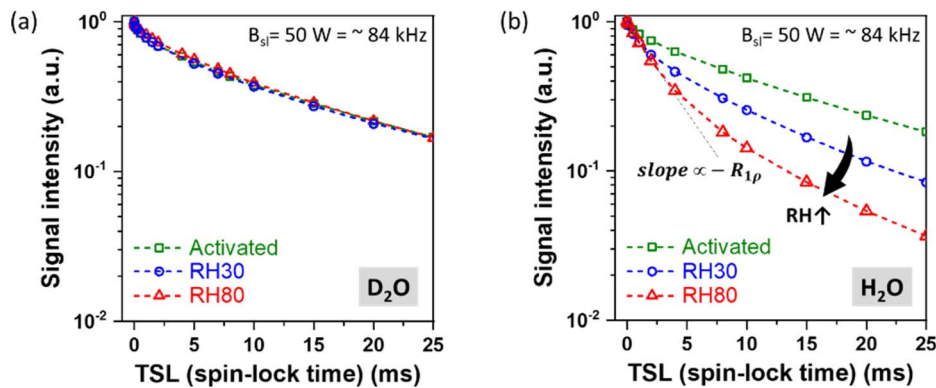


Fig. 8  $^1\text{H}$  NMR relaxation decay curves obtained at 9.4 T of activated and water vapor (including  $\text{N}_2$ , using either (a)  $\text{D}_2\text{O}$  or (b)  $\text{H}_2\text{O}$ ) adsorbed materials at 25  $^\circ\text{C}$  with RH30, and RH80 for  $R_1 (=1/T_1)$  relaxations. Considering potential deuterium exchange in polymer, the data presented in  $\text{D}_2\text{O}$  is used after reactivating  $\text{D}_2\text{O}$  adsorbed sample in (a).

1 adsorption sites or pathways, thereby impeding CO<sub>2</sub> adsorption  
at 80% RH. This observation aligns with the general trend of  
increased water sorption at high RH levels,<sup>36,47</sup> where water  
sorption escalates from monolayer to multilayer, and eventually  
5 leading to capillary condensation of water molecules.<sup>47</sup>  
Furthermore, a similar transition from enhanced adsorptive to  
competitive behavior with increasing RH has also been  
observed in other studies using FTIR. Indeed, FTIR study on  
polyimide covalent organic frameworks further has identified  
10 peaks corresponding to water uptake at varying RH levels and  
highlighting water molecules readily occupy adsorption sites,  
suggesting a strong affinity for water adsorption at higher RH  
values (around 38–42% RH) in H<sub>2</sub>O–CO<sub>2</sub> adsorption.<sup>36</sup>

15 We conclude that increasing RH induces pore swelling,  
concomitant with a significant increase in water adsorption.  
This leads to a complex interplay between CO<sub>2</sub> and H<sub>2</sub>O  
adsorption, impacting adsorption capacity. This corroborates  
the dominant CO<sub>2</sub> adsorption over H<sub>2</sub>O adsorption at 30% RH,  
20 as observed in the enhanced CO<sub>2</sub> uptake in both the isotherm  
experiment and NMR experiment.<sup>25</sup> At 30% RH, when only  
tightly bound water adsorption or only a few more layers may  
compete with CO<sub>2</sub> in the swollen pores, the CO<sub>2</sub> adsorption  
capacity is enhanced. Conversely, at 80% RH, the substantial  
25 amount of water adsorption likely attracts more water and  
reduces CO<sub>2</sub> adsorption capacity despite the expanded pores  
within the sorbent. Finally, lubrication of molecular motion for  
both the polymer and bound water occurs with increasing RH  
exposure.

## 30 Conclusions

The CO<sub>2</sub> adsorption behavior in polymer resin Lewatit® VP OC  
1065 for DAC applications was investigated using solid-state  
35 NMR. The CO<sub>2</sub> partial pressure and the relative humidity were  
found to be key factors influencing the sorption. In the absence  
of water, the effect of CO<sub>2</sub> partial pressure on both chemisorption  
and physisorption processes highlights a stepwise process  
characterized by the sequential formation of ammonium  
40 carbamate, carbamic acid, and ultimately physisorption, all  
contingent upon the CO<sub>2</sub> loading levels. Additionally, the relative  
humidity at low CO<sub>2</sub> loadings influences total CO<sub>2</sub> sorption,  
with increased sorption capacity at 30% RH, and decreased CO<sub>2</sub>  
sorption capacity at 80% RH. At the low CO<sub>2</sub> partial pressures,  
45 however, we found that the RH does not change the CO<sub>2</sub>–amine  
binding mechanism, even while changing the overall CO<sub>2</sub>  
uptake; this is in contrast with previous studies theorizing the  
formation of bicarbonate species thereby improving the stoi-  
chiometry. Bicarbonate is not observed in any of the experi-  
50 ments undertaken here.

Instead, we found that the impact of water on CO<sub>2</sub> uptake is  
accounted for by considering the molecular dynamics of water  
and the surrounding sorbent polymer induced by water  
55 adsorption. We assert that the adsorption of water into the  
pores leads to pore expansion over time, opening migration  
pathways and thereby increasing the availability of CO<sub>2</sub> sorption  
sites (*i.e.*, amino groups). The specific RH levels affect the extent  
of pore expansion and local water molecular motion. Two

1 distinct NMR relaxation regimes suggest a transition from water  
molecules that are tightly bound or form only a few layers on the  
adsorbate at 30% RH to water molecules that exhibit capillary  
condensation and include more multilayered structures at 80%  
5 RH. This observation likely contributes to variations in CO<sub>2</sub>  
adsorption capacity under different RH conditions, with corre-  
sponding changes in the relaxation rates.

Our analysis conclusively shows that, in ultra dilute CO<sub>2</sub>  
streams, the effect of water on CO<sub>2</sub> adsorption is not chemical  
but physical. Specifically, our findings contribute to under-  
10 standing the underlying water/carbon dioxide co-adsorption  
phenomena in amine-modified polymer resins. The presence  
of water induces the pore opening due to polymer swelling and  
thereby affecting CO<sub>2</sub> sorption without altering the chemical  
reaction route. These insights are critical to underpin optimized  
15 DAC materials and process designs moving forward. Finally, the  
experimental framework demonstrated here allows future  
studies to address the same questions for other amine-modified  
DAC adsorbents classes.

## Experimental methods

### Sample preparation and NMR analysis under dry and wet 20 conditions

The sorbent material used in this study, Lewatit® VP OC 1065,  
25 underwent activation by heating at 100 °C under ultra-high  
vacuum ( $\sim 10^{-3}$  torr) for several hours before gas adsorption.  
Subsequently, the activated samples were subjected to both dry  
and wet conditions.

For dry adsorption experiments, the activated samples in the  
packed rotor were subjected to varying partial pressures of  
30 <sup>13</sup>CO<sub>2</sub> (Sigma-Aldrich carbon-<sup>13</sup>C dioxide <3 atom% <sup>18</sup>O, 99.0  
atom% <sup>13</sup>C) using a home-built *ex situ* dry gas apparatus. The  
partial pressures used were 8, 35, and approximately 1000 mbar,  
35 and each adsorption lasted for one hour. NMR experiments for  
the dry gas adsorbed samples were carried out at 11.75 T using  
a Bruker 4 mm dual-channel CPMAS probe. <sup>13</sup>C MAS NMR  
spectra were acquired at room temperature with a MAS rate of  
40 10 kHz. The <sup>1</sup>H → <sup>13</sup>C cross-polarization (CP) transfer under  
MAS (CPMAS) experiments were obtained with a contact time of  
 $\tau_{CP} = 2$  ms, during which a constant RF-field equal to 52 kHz  
was applied on the <sup>13</sup>C, while the <sup>1</sup>H RF-field amplitude was  
45 linearly ramped from 30 to 59 kHz. During <sup>13</sup>C acquisition,  
high-power <sup>1</sup>H decoupling was applied using the two-pulse  
phase-modulated (tpm15) decoupling scheme with an RF-  
field amplitude set to 50 kHz.<sup>48</sup> A total of 128–2k transients  
were averaged with a repetition time of 2 s.

The 2D <sup>1</sup>H–<sup>13</sup>C CP-based heteronuclear correlation (CP-  
50 HETCOR) spectra were acquired using a contact time of 50  $\mu$ s  
and 70 kHz of on-resonance frequency switched Lee-Goldberg  
(FSLG) homonuclear decoupling during the  $t_1$  evolution  
period.<sup>49</sup> During <sup>13</sup>C acquisition, high-power <sup>1</sup>H decoupling was  
55 applied using the tpm 15 decoupling scheme with an RF-field  
amplitude set to 50 kHz. In total, 80  $t_1$  increments were recor-  
ded ( $\Delta t = 26.95$   $\mu$ s), each made of 200 transients with a repeti-  
tion time of 2 s, leading to an overall experimental time of  $\sim 9$   
hours.

1 Direct excitation carbon spectra were acquired using high-  
power  $^1\text{H}$  decoupling was applied using the tppm 15 decou-  
pling scheme with an RF-field amplitude set to 25–50 kHz. They  
5 were employed to probe physisorbed  $\text{CO}_2$  and quantify carbon  
in the adsorbed samples with a recycle delay of 2 s and 120 s  
with 16–2k and 256 transients, respectively. The chemical shift  
anisotropy (CSA) tensors were estimated from the low-speed  
MAS  $^{13}\text{C}$  spectra collected at a MAS rate of 3 kHz with  
10 a recycle delay of 120 s. The spectral deconvolutions were per-  
formed using Dmfit software.<sup>50</sup>

Under humid conditions at a controlled low partial pressure  
of  $\text{CO}_2$ , the activated samples were loaded into an *ex situ* co-  
adsorption apparatus, where the partial pressure of  $^{13}\text{CO}_2$  in  
the gas mixture and the amount of  $\text{H}_2\text{O}$  vapor precisely  
15 controlled by manipulating their flow rates. Relative humidity  
(RH) levels of 0%, 30%, and 80% were explored, with each  
adsorption lasting 3–4 hours. NMR experiments discussed for  
the humid gas adsorbed samples were conducted at 9.4 T,  
monitoring at a MAS rate of 10 kHz using a Bruker 3.2 mm  
20 probe. A rotor-synchronized DEPTH pulse was employed to  
suppress background  $^1\text{H}$  signals.<sup>51</sup>  $^{13}\text{C}$  CPMAS spectra were  
measured with a contact time of  $\tau_{\text{CP}} = 0.2$  ms, during which  
a constant RF-field equal to 61 kHz was applied on the  $^{13}\text{C}$ ,  
25 while the  $^1\text{H}$  RF-field amplitude was linearly ramped from 71  
to 89 kHz. During  $^{13}\text{C}$  acquisition, high-power  $^1\text{H}$  decoupling  
was applied using Small Phase Incremental Alternation with 64  
steps (SPINAL-64) decoupling scheme with an RF-field ampli-  
tude set to 89 kHz.<sup>52</sup> A total of 2k–4k transients were averaged  
30 with a repetition time of 1.5–2 s resulting in experimental times  
of 1–2 hours. Carbon quantification was accomplished by direct  
excitation with SPINAL-64 decoupling scheme set to 89 kHz. A  
total of 160 transients were averaged with a recycle delay of 140 s  
resulting into 6 hours and 13 min experimental time. Addition-  
35 ally, 2D  $^1\text{H}$ – $^{13}\text{C}$  HETCOR spectra were recorded with  
a contact time of 200  $\mu\text{s}$  during the CP transfer and FSLG  
of around 89 kHz during  $^1\text{H}$  evolution period while keeping the  
rest of CP parameters. In total, 64  $t_1$  increments were recorded  
( $\Delta t = 44.8625$   $\mu\text{s}$ ), each made of 16–512 transients with a repe-  
40 tition time of 1.5–2 s resulting in experimental times of 0.5–12  
hours.

For all 2D HETCOR spectra under dry and wet conditions,  
proton chemical shifts were referenced by  $^1\text{H}$ – $^1\text{H}$  FSLG pulse  
45 sequence immediately after acquiring the 2D HETCOR without  
altering any parameters.<sup>53</sup> Short cross-polarization contact  
times (50  $\mu\text{s}$ ) were used throughout this work to emphasize  
carbon-13 peaks proximate to protons, albeit at a significant  
loss of signal-to-noise. For 2D HETCOR experiments dosed at  
50 150 ppm  $\text{CO}_2$ , the contact time was increased to 200  $\mu\text{s}$   
to improve sensitivity.

$R_2$  and  $R_{1\rho}$  relaxation measurements at 9.4 T were performed  
at room temperature.  $R_2$  relaxation was conducted by using  
a rotor synchronized spin-echo pulse sequence with a spinning  
55 rate of 20 kHz. Echo time were varied from 100  $\mu\text{s}$  up to around  
10 ms with a time interval of 100 to 200  $\mu\text{s}$ .  $R_{1\rho}$  relaxation  
measured at a MAS rate of 10 kHz was collected with the  
sequence consisting of  $90^\circ$  excitation pulse followed with  
a spin-locking time (TSL) from 50  $\mu\text{s}$  to 20 ms, using 12 to 16

1 TSL points with a spin-locking field strength of around 84 kHz  
1 followed by a rotor-synchronized spin echo detection (using  
180° refocusing pulse).

The  $\text{D}_2\text{O}$  adsorption experiments were conducted to investi-  
5 gate the interaction between deuterium oxide and activated  
materials, with a specific focus on revealing the molecular  
dynamics of water and its impact on the sorbent resin. Nitrogen  
( $\text{N}_2$ ) was chosen as the carrier gas and was directed through  
10 a bubbler containing  $\text{D}_2\text{O}$  to saturate the gas with  $\text{D}_2\text{O}$  vapor,  
achieving the targeted relative humidity level. To maintain  
consistency with parallel experiments conducted under similar  
humid conditions, the duration of  $\text{D}_2\text{O}$  exposure was adjusted  
15 accordingly, ensuring uniform exposure times across all  
experiments.

$^1\text{H}$  and  $^{13}\text{C}$  chemical shift were referenced with respect to  
15 tetramethylsilane using the  $\text{CH}_2$  resonance of adamantane as  
a secondary external reference at  $\delta_{\text{iso}}(^{13}\text{C}) = 38.48$  ppm and  $\delta_{\text{iso}}$   
( $^1\text{H}$ ) = 1.8 ppm.

### Low magnetic field transverse relaxation measurement ( $R_2$ )

This experiment aims to measure the swelling of Lewatit® VP  
20 OC 1065 in  $\text{H}_2\text{O}$  using low magnetic field  $^1\text{H}$   $T_2$  relaxation at  
room temperature. The 0.3 T unilateral magnet NMR-MOUSE  
(MOBILE Universal Surface Explorer) PM25 was interfaced to  
25 a Magritek Kea II spectrometer to detect transverse relaxation of  
the polymer over 3 hours, during which time 52 CPMGs were  
recorded.<sup>54–58</sup> For all experiments,  $\pi/2$  pulse lengths were 2.5  $\mu\text{s}$   
and the repetition time for signal averaging was 10 s. A total of  
1000 echoes separated by a delay of 55  $\mu\text{s}$  were recorded, and  
30 128 scans were signal averaged. To cancel artifacts arising from  
pulse imperfections, the initial  $\pi/2$  rf pulse and the receiver  
were phase cycled between  $+x$  and  $-x$  while holding the  $\pi$  rf  
pulse phase constant at  $+y$ . Inversion of the multiexponential  
35 time decay to a distribution of  $R_2$  was accomplished with Lap-  
lace inversion using the Lawson and Hanson algorithm in  
Prosop software v3.61.<sup>59,60</sup> A smoothing value of 0.9 was chosen  
by minimizing  $\chi^2$  without oversmoothing.

These experiments detect two significant  $R_2$  relaxation rates,  
40 and the shorter  $T_2$  relaxation time is attributed to water imbibed  
within the porous polymer network. Subsequent observation of  
the polymer swelling over 24 hours was detected in a similar  
way.

### Adsorption isotherm experiments and the calculation of the isosteric heat of adsorption

Single and binary component  $\text{CO}_2$  and water isotherms for  
50 Lewatit were measured using the DVS Vacuum system from  
Surface Measurement Systems. The DVS uses a gravimetric  
magnetic suspension balance to measure the mass of the  
sample throughout adsorption and desorption. Samples of  
between 30–60 mg were first outgassed in the DVS at a temper-  
55 ature of 100 °C. A turbomolecular pump was used to achieve  
pressures of  $10^{-5}$  bar and ensure thorough outgassing of the  
sample prior to adsorption. Once the sample was outgassed and  
the system was brought down to the adsorption temperature,  
the pressure of adsorbate was increased stepwise, and the mass

was allowed to equilibrate before moving to the next pressure step. Desorption branches were similarly obtained by decreasing the pressure in the same stepwise manner. The DVS can operate in dynamic or static mode. Dynamic mode is when the gas/vapour flows through the chamber whereas static mode is when the gas is pulsed into the chamber. Water isotherms were measured using dynamic mode and CO<sub>2</sub> isotherms were measured using static mode.

Co-adsorption isotherms were measured using semi-static mode. For these measurements, Lewatit was outgassed as above and the first adsorption step pre-adsorbed the sample with water at a determined relative humidity while the following pressure doses were CO<sub>2</sub>. Working under the assumption that

CO<sub>2</sub> does not affect water adsorption,<sup>10</sup> subsequent mass increases were attributed to CO<sub>2</sub> adsorption. Desorption was not performed for co-adsorption experiments as there is

currently no way to differentiate between water and CO<sub>2</sub> desorption in the DVS.

The isosteric heat of adsorption was calculated using the Clausius–Clapeyron equation. The heat of adsorption across many different CO<sub>2</sub> loadings was obtained by interpolating the isotherms.

## Data availability

All data supporting the findings of this study are available within the main article and the electronic ESI.† All raw NMR data have been deposited on Dryad at <https://doi.org/10.5061/dryad.h70rxwdsx>.

## Author contributions

A. S. conceived and designed the research, conducted experiments and analysis, and wrote the original draft. J. Y. performed the measurement of adsorption isotherms and participated in discussion. J. W. and S. N. F. conducted *R*<sub>2</sub> measurements at low magnetic field and analyzed the data. K. P., S. G., and M. v. S. participated in discussions and offered valuable comments and experimental analyses. R. G. assisted with setting NMR pulses and participated in discussion. All authors edited the manuscript. J. A. R. supervised the research.

## Conflicts of interest

There are no conflicts to declare.

## Acknowledgements

We thank Dr Hasan Celik, and Pines Magnetic Resonance Center's Core NMR Facility (PMRC Core) for spectroscopic assistance. This work is part of PrISMa Project (No. 299659), funded through the ACT programme (Accelerating CCS Technologies, Horizon2020 Project No. 294766). Financial contributions made from the Department for Business, Energy & Industrial Strategy (BEIS) together with extra funding from the NERC and EPSRC research councils, United Kingdom; The Research Council of Norway (RCN), Norway; the Swiss Federal Office of Energy (SFOE), Switzerland; and the US-Department of Energy (US-DOE), USA, are gratefully acknowledged. Additional financial support from TOTAL and Equinor is also gratefully acknowledged. We also acknowledge funding from the USorb-DAC Project, supported by a grant from The Grantham Foundation for the Protection of the Environment to RMI's climate tech accelerator

NERC and EPSRC research councils, United Kingdom; The Research Council of Norway, (RCN), Norway; the Swiss Federal Office of Energy (SFOE), Switzerland; and the US-Department of Energy (US-DOE), USA, are gratefully acknowledged. We thank Drs Hasan Celik, and Pines Magnetic Resonance Center's Core NMR Facility (PMRC Core) for spectroscopic assistance. The instrument used in this work is supported by the National Science Foundation under Grant No. 2018784.

## Notes and references

- 1 M. A. Caretta, A. Mukherji, M. Arfanuzzaman, R. A. Betts, A. Gelfan, Y. Hirabayashi, T. K. Lissner, J. Liu, E. Lopez Gunn, R. Morgan, S. Mwangi, and S. Supratid, in *Climate Change 2022: Impacts, Adaptation, and Vulnerability*, Cambridge, UK and New York, NY, USA, pp. , pp. 551–712.
- 2 S. Sanz-Pérez, C. R. Murdock, S. A. Didas and C. W. Jones, *Chem. Rev.*, 2016, **116**, 11840–11876.
- 3 R. Bergman and A. Anatoly, *The Case for Carbon Dioxide Removal: From Science to Justice*, Carbon Dioxide Removal Primer, CDR Primer.
- 4 A. Sodiq, Y. Abdullatif, B. Aissa, A. Ostovar, N. Nassar, M. El-Naas and A. Amhamed, *Environ. Technol. Innovation*, 2023, **29**, 102991.
- 5 J. F. Wiegner, A. Grimm, L. Weimann and M. Gazzani, *Ind. Eng. Chem. Res.*, 2022, **61**, 12649–12667.
- 6 M. Sendi, M. Bui, N. Mac Dowell and P. Fennell, *One Earth*, 2022, **5**, 1153–1164.
- 7 L. Küng, S. Aeschlimann, C. Charalambous, F. McIlwaine, J. Young, N. Shannon, K. Strassel, C. N. Maesano, R. Kahsar, D. Pike, M. van der Spek and S. Garcia, *Energy Environ. Sci.*, 2023, **16**, 4280–4304.
- 8 M. W. Hahn, M. Steib, A. Jentyts and J. A. Lercher, *J. Phys. Chem. C*, 2015, **119**, 4126–4135.
- 9 H. Zhang, A. Goepfert, G. K. S. Prakash and G. Olah, *RSC Adv.*, 2015, **5**, 52550–52562.
- 10 R. Veneman, N. Frigka, W. Zhao, Z. Li, S. Kersten and W. Brilman, *Int. J. Greenh. Gas Control*, 2015, **41**, 268–275.
- 11 R. Serna-Guerrero, E. Da'na and A. Sayari, *Ind. Eng. Chem. Res.*, 2008, **47**, 9406–9412.
- 12 R. A. Khatri, S. S. C. Chuang, Y. Soong and M. Gray, *Energy Fuels*, 2006, **20**, 1514–1520.
- 13 J. Yu and S. S. C. Chuang, *Energy Fuels*, 2016, **30**, 7579–7587.
- 14 S. A. Didas, M. A. Sakwa-Novak, G. S. Foo, C. Sievers and C. W. Jones, *J. Phys. Chem. Lett.*, 2014, **5**, 4194–4200.
- 15 K. Li, J. D. Kress and D. S. Mebane, *J. Phys. Chem. C*, 2016, **120**, 23683–23691.
- 16 G. A. Russell-Parks, N. Leick, M. A. T. Marple, N. A. Strange, B. G. Trewyn, S. H. Pang and W. A. Braunecker, *J. Phys. Chem. C*, 2023, **127**, 15363–15374.
- 17 Z. Bacsik, N. Ahlsten, A. Ziadi, G. Zhao, A. E. Garcia-Bennett, B. Martín-Matute and N. Hedin, *Langmuir*, 2011, **27**, 11118–11128.
- 18 N. Hedin and Z. Bacsik, *Curr. Opin. Green Sustainable Chem.*, 2019, **16**, 13–19.
- 19 M. Parvazinia, S. Garcia and M. Maroto-Valer, *Chem. Eng. J.*, 2018, **331**, 335–342.



- 20 W. R. Alesi Jr and J. R. Kitchin, *Ind. Eng. Chem. Res.*, 2012, **51**, 6907–6915.
- 21 W. Buijs, *Ind. Eng. Chem. Res.*, 2019, **58**, 17760–17767.
- 22 A. P. Hallenbeck and J. R. Kitchin, *Ind. Eng. Chem. Res.*, 2013, **52**, 10788–10794.
- 23 Q. Yu, J. de la, P. Delgado, R. Veneman and D. W. F. Brillman, *Ind. Eng. Chem. Res.*, 2017, **56**, 3259–3269.
- 24 W. Buijs and S. de Flart, *Ind. Eng. Chem. Res.*, 2017, **56**, 12297–12304.
- 25 J. Young, E. García-Díez, S. Garcia and M. van der Spek, *Energy Environ. Sci.*, 2021, **14**, 5377–5394.
- 26 H. Mao, J. Tang, G. S. Day, Y. Peng, H. Wang, X. Xiao, Y. Yang, Y. Jiang, S. Chen, D. M. Halat, A. Lund, X. Lv, W. Zhang, C. Yang, Z. Lin, H.-C. Zhou, A. Pines, Y. Cui and J. A. Reimer, *Sci. Adv.*, 2022, **8**, eabo6849.
- 27 J. Herzfeld and A. E. Berger, *J. Chem. Phys.*, 1980, **73**, 6021–6030.
- 28 Z. Gu and A. McDermott, *J. Am. Chem. Soc.*, 1993, **115**, 4282–4285.
- 29 T. Čendak, L. Sequeira, M. Sardo, A. Valente, M. L. Pinto and L. Mafra, *Chem.–Eur. J.*, 2018, **24**, 10136–10145.
- 30 J. M. Kolle, M. Fayaz and A. Sayari, *Chem. Rev.*, 2021, **121**, 7280–7345.
- 31 R. B. Said, J. M. Kolle, K. Essalah, B. Tangour and A. Sayari, *ACS Omega*, 2020, **5**, 26125–26133.
- 32 P. V. Kortunov, M. Siskin, L. S. Baugh and D. C. Calabro, *Energy Fuels*, 2015, **29**, 5919–5939.
- 33 Y. F. Chen, R. Babarao, S. I. Sandler and J. W. Jiang, *Langmuir*, 2010, **26**, 8743–8750.
- 34 F. Brandani and D. M. Ruthven, *Ind. Eng. Chem. Res.*, 2004, **43**, 8339–8344.
- 35 C. Y. Chuah, W. Li, Y. Yang and T.-H. Bae, *Chem. Eng. J. Adv.*, 2020, **3**, 100021.
- 36 H. Veldhuizen, S. A. Butt, A. Van Leuken, B. Van Der Linden, W. Rook, S. Van Der Zwaag and M. A. Van Der Veen, *ACS Appl. Mater. Interfaces*, 2023, **15**, 29186–29194.
- 37 J. Hack, N. Maeda and D. M. Meier, *ACS Omega*, 2022, **7**, 39520–39530.
- 38 C.-H. Chen, D. Shimon, J. J. Lee, F. Mentink-Vigier, I. Hung, C. Sievers, C. W. Jones and S. E. Hayes, *J. Am. Chem. Soc.*, 2018, **140**, 8648–8651.
- 39 C.-H. Chen, E. L. Sesti, J. J. Lee, F. Mentink-Vigier, C. Sievers, C. W. Jones and S. E. Hayes, *J. Phys. Chem. C*, 2021, **125**, 16759–16765.
- 40 N. Bloembergen, E. M. Purcell and R. V. Pound, *Phys. Rev.*, 1948, **73**, 679–712.
- 41 M. H. Levitt, *Spin Dynamics: Basics of Nuclear Magnetic Resonance*, John Wiley & Sons, 2013.
- 42 L. R. Stingaciu, A. Pohlmeier, P. Blümmler, L. Weihermüller, D. van Dusschoten, S. Stapf and H. Vereecken, *Water Resour. Res.*,
- 43 P. J. Barrie, in *Annual Reports on NMR Spectroscopy*, Academic Press, 2000, vol. 41, pp. 265–316.
- 44 Z. Zhao, B. Wang, R. Tan, W. Liu and M. Zhang, *Magn. Reson. Chem.*, 2022, **60**, 427–433.
- 45 Y. Aso, S. Yoshioka, J. Zhang and G. Zograf, *Chem. Pharm. Bull.*, 2002, **50**, 822–826.
- 46 B. Wiesner, B. Kohn, M. Mende and U. Scheler, *Polymers*, 2018, **10**, 1231.
- 47 X. Ma, W. Shen, X. Li, Y. Hu, X. Liu and X. Lu, *Sci. Rep.*, 2020, **10**, 13434.
- 48 A. E. Bennett, C. M. Rienstra, M. Auger, K. V. Lakshmi and R. G. Griffin, *J. Chem. Phys.*, 1995, **103**, 6951–6958.
- 49 B.-J. van Rossum, H. Förster and H. J. M. de Groot, *J. Magn. Reson.*, 1997, **124**, 516–519.
- 50 D. Massiot, F. Fayon, M. Capron, I. King, S. Le Calvé, B. Alonso, J.-O. Durand, B. Bujoli, Z. Gan and G. Hoatson, *Magn. Reson. Chem.*, 2002, **40**, 70–76.
- 51 D. G. Cory and W. M. Ritchey, *J. Magn. Reson.*, 1988, **80**, 128–132.
- 52 B. M. Fung, A. K. Khitrin and K. Ermolaev, *J. Magn. Reson.*, 2000, **142**, 97–101.
- 53 B. Kumari, M. Brodrecht, T. Gutmann, H. Breitzke and G. Buntkowsky, *Appl. Magn. Reson.*, 2019, **50**, 1399–1407.
- 54 B. Blümich and J. Anders, *Magn. Reson.*, 2021, **2**, 149–160.
- 55 J. Perlo, F. Casanova and B. Blümich, *J. Magn. Reson.*, 2005, **176**, 64–70.
- 56 G. Eidmann, R. Savelsberg, P. Blümmler and B. Blümich, *J. Magn. Reson., Ser. A*, 1996, **122**, 104–109.
- 57 H. Y. Carr and E. M. Purcell, *Phys. Rev.*, 1954, **94**, 630–638.
- 58 S. Meiboom and D. Gill, *Rev. Sci. Instrum.*, 1958, **29**, 688–691.
- 59 C. L. Lawson and R. J. Hanson, *Solving Least Squares Problems*, Prentice-Hall, Englewood Cliffs, NJ, 1974.
- 60 R. F. Ling, *J. Am. Stat. Assoc.*, 1977, **72**, 930–931.
- 61 A. Song, J. Young, J. Wang, S. N. Fricke, K. Piscina, R. Giovine, S. Garcia, M. Spek and J. A. Reimer, *Dryad*, 2024, DOI: <https://doi.org/10.5061/dryad.h70rxwdsx>.